Observation of currentless redox reactions on surface of water jet immersed in low-pressure plasma

Takeshi Ito[1], **Tetsuo Sakka**[2], **and Koichi Sasaki**[1]

[1]Division of Applied Quantum Science and Engineering, Hokkaido University, Sapporo 060-8628, Japan

[2]Department of Energy and Hydrocarbon Chemistry, Kyoto University, Kyoto 615-8510, Japan

E-mail: sasaki@qe.eng.hokudai.ac.jp

Abstract. We investigated oxidation-reduction reactions on the surface of water jet immersed in a low-pressure inductively coupled helium plasma. The electrical potential of the water jet was floating, and no electrical current was supplied from the plasma to the water jet. We observed the productions of molecular hydrogen and molecular oxygen. We also observed negligible consumption of water vapor in the gas phase, suggesting that the productions of hydrogen and oxygen were not owing to the conversion from water vapor. When we employed silver nitrate solution instead of pure water, we observed the decrease in the production rate of hydrogen, whereas the production rate of oxygen was the same in pure water and silver nitrate solution. In addition, we found the synthesis of silver particulates in the silver nitrate solution, indicating the competition between the reductions of H^+ and Ag^+. Thus, the experimental results reveal the simultaneous oxidation and reduction at the same plasma-liquid interface.

Electrochemistry or electrolysis utilizes reactions induced by the transfer of electrons at the interfaces between solid electrodes and solution. The electrodes for oxidation and reduction are separated in usual electrolysis, and they are called the anode and the cathode, respectively. Electrons are provided from a reactant (reductant) on the anode, resulting in an oxidation reaction, whereas the cathode provides electrons to a reactant (oxidant), resulting in a reduction reaction. An external power supply is necessary to keep the electrolysis reaction. The voltage between the anode and the cathode must exceed the redox potential difference, which is 1.23 eV for water oxidation to O_2 with respect to water reduction to H_2.

Recently, many researchers report plasma-assisted electrolysis, where one or both of the electrodes are replaced with atmospheric-pressure plasmas [1]. The difference between the plasma-assisted and conventional electrolyses is summarized as follows; 1) the plasma-assisted electrolysis can utilize the interface between gas (plasma) and solution for redox reactions [2, 3], 2) electrons can have kinetic energy if the plasma works as the cathode [4–7], and 3) ions and neutral radicals are transported from the plasma in addition to electrons [8–10]. We can obtain various nanoparticles of metals [11–14] and oxides [15–17] in a form of suspension by plasma-assisted electrolysis. The synthesis of nanoparticles is owing to the reduction of metal cations by the reaction with electrons, but the contribution of atomic

hydrogen transported from the plasma is discussed in some papers [18–20]. The plasma-assisted electrolysis opens a new aspect of electrochemistry. However, all the experiments of plasma-assisted electrolysis keep the situations with the separated interfaces (electrodes) for oxidation and reduction.

In this paper, we report oxidation and reduction on a water surface immersed in a low-pressure plasma. The reason for the use of a low-pressure plasma instead of an atmospheric-pressure plasma is that it is more suitable to quantitative experiment since the measurements of the plasma density and the composition of gas-phase species are easier. The difficulty that is caused by the high vapor pressure of water is solved by employing water in the form of a slender jet, a turbomolecular pump with a high pumping speed, and water traps at the temperature of liquid nitrogen [21–24]. A point of this work is that we did not use the typical geometry of electrochemistry. We observed oxidation and reduction on the surface of the same water jet immersed in a low-pressure plasma.

Figure 1 shows the schematic of the experimental apparatus. Purified water with an electrical conductance less than 0.01 mS/cm was stored in a glass beaker, and it was supplied to a plastic nozzle through a plastic tube at a flow rate of 1.6 mL/min using a plunger pump. The plunger pump was electrically floating using an isolation transformer. The diameter of the nozzle was 50 μm. The inside pressure of the nozzle was so high that water was ejected from the nozzle in the form of a jet. The water jet system was installed at the top of a vacuum chamber, and the water passing through the chamber was caught at the bottom of the chamber using a tank at the temperature of liquid nitrogen. The distance between the nozzle and the tank was approximately 50 cm. The water jet was switched on before starting the evacuation of the vacuum chamber, otherwise the static water inside the nozzle was frozen by the latent heat of vaporization. We employed a turbomolecular pump with a pumping speed of 2000 L/s. In addition to the high-speed pump, we installed a water vapor trap at the temperature of liquid nitrogen to reduce the pressure of water vapor in the chamber. By using this evacuation system, we realized 2.0 mTorr for the pressure of water vapor in the chamber. The water jet was stable and had a length of 20 cm in air, but it was dispersed into droplets during the flight in vacuum. The length of the water jet in vacuum was approximately 10 mm and it did not reach the water tank. Therefore, the potential of the water jet was floating and we did not have current through the water jet. We used a silver nitrate solution with a concentration of 0.1 M instead of pure water in an experiment for comparison. In addition, we carried out a comparative experiment without the water jet (but with water vapor), where we connected a small container with liquid water to the plasma chamber. Note that the liquid water in the container was not in contact with the plasma. The flow rate of water vapor was controlled by the temperature of the container and the conductance of a needle valve, and the pressure of water vapor was adjusted at the same pressure of 2.0 mTorr. The liquid nitrogen-cooled water tank and the water vapor trap were activated, and the evacuation speed in the comparative experiment was the same as that in the water-jet experiment. The role of the comparative experiments was to verify the plasma-induced redox reactions on the surface of the water jet.

After completing the evacuation, we introduced helium into the vacuum chamber at a flow rate of 355 sccm. The reason for the use of helium was its boiling temperature lower than

the temperature of liquid nitrogen. The partial pressure of helium was 10 mTorr. The plasma was produced by inductively coupled discharge at 13.56 MHz. The rf power was supplied to a 2.5-turn rf antenna wound around the glass tube of 8.5 cm diameter via a matching circuit. The distance between the rf antenna and the water jet was approximately 70 mm. The H-mode discharge was observed at the present experimental condition. We used a Langmuir double probe for measuring the plasma density and the electron temperature. The probe was positioned at a distance of 10 mm from the water jet. The plasma density was approximately proportional to the rf power, whereas the electron temperature was ~ 4 eV and was roughly independent of the rf power.

We installed a quadrupole mass spectrometer (QMS) in another vacuum chamber. The QMS chamber, which was connected to the plasma chamber via an orifice with a diameter of 0.5 mm, was positioned at the counter side of the rf discharge system, as shown in Fig. 1. The distance between the orifice and the water jet was 17 mm. The QMS chamber was differentially evacuated using a turbomolecular pump below 10^{-6} Torr. The orifice to extract the gas in the plasma was covered with grounded aluminum plate, by which we avoided the direct transport of positive ions in the plasma to the secondary electron multiplier in QMS. To evaluate the production rates of molecular hydrogen and molecular oxygen, we introduced hydrogen or oxygen gas into the plasma at an arbitrary flow rate. We obtained the relationships (the calibration curves) between the flow rates and the increases in the QMS signals at $m/z = 2$ and 32, and they were used for evaluating the production rates in the plasma. The decomposition (or the production) rate of water vapor was evaluated from the decrease (or the increase) in the QMS signal at $m/z = 18$ with the help of the evaporation rate of the liquid water. The evaporation rate of water was estimated to be 80 μmol/s from the decrease in the volume of water in the container used in the comparative experiment. We observed the change in the QMS signal of helium when we changed the rf power, which was understood to be due to the variation in the gas temperature. In this case, we normalized the QMS signals at $m/z = 2$, 18, and 32 by the ratio of the change in the helium signal to compensate the variation in the gas temperature.

Figures 2(a) and 2(b) show the mass spectra we observed in the absence and presence of the plasma, respectively. The water jet was immersed in the plasma at an rf power of 120 W. As shown in the figure, we observed significant increases in the densities of molecular hydrogen and molecular oxygen by producing the plasma. In addition, we also observed the increase in the water vapor density. The similar mass spectra we observed in the comparative experiment using the water vapor injection are shown in Figs. 2(c) and 2(d). We also observed the increases in the densities of molecular hydrogen and molecular oxygen in the comparative experiment. A remarkable difference from the results observed using the water jet was the decrease in the water vapor density by the plasma production.

The production rates of molecular hydrogen, molecular oxygen, and water vapor are plotted in Fig. 3 as a function of the plasma density. The plasma density was varied by changing the rf power with keeping the helium pressure. Figure 3(a) was obtained when we used the water jet, while only water vapor was injected into the chamber in Fig. 3(b). The plasma densities were almost the same in Figs. 3(a) and 3(b) at the same rf powers.

The production rates of molecular hydrogen and molecular oxygen were proportional to the plasma density, as shown in Fig. 3. The production rates of molecular oxygen were almost the same in Figs. 3(a) and 3(b), whereas the production rate of molecular hydrogen when using the water jet was higher than that using the water vapor injection. In addition, the half of the production rate of hydrogen was higher than the production rate of oxygen. The vaporization rates of water vapor were significantly different in Figs. 3(a) and 3(b). We observed the negative rate, *i.e.*, the loss of water vapor, in the experiment using the water vapor injection, as shown in Fig. 3(b). In contrast, in the experiment using the water jet, we observed the increase in the water vapor density as a function of the plasma density, as shown in Fig. 3(a).

The sputtering of the water jet surface was negligible since the plasma potential ($\sim$ 15 V) was much lower than the threshold energy. Hence, the mechanism for the production of water vapor in the water jet experiment was considered to be the increase in the vaporization pressure of the water jet due to the rise in the temperature, and we measured the temperature of the joint just above the nozzle using a thermocouple at each rf power. As a result, we observed the increase of 1-7 K at rf powers between 80 and 140 W. We assumed the same temperature rise for water as the upper limit estimation, and we evaluated the increase in the vaporization pressure. The temperature of the water jet after the ejection into the vacuum was estimated by

$$\frac{\mathrm{d}T(z)}{\mathrm{d}z} = -2\frac{r'}{v_{\mathrm{jet}}}\frac{L}{c_{\mathrm{p}}}\frac{1}{r_0}\sqrt{\frac{T(z)}{T_{\mathrm{ref}}}}\exp\left[-\frac{L}{kT_{\mathrm{ref}}}\left(\frac{T_{\mathrm{ref}}-T(z)}{T(z)}\right)\right], \tag{1}$$

where z and r_0 are the distance from the nozzle along the jet axis and the jet radius, respectively, $r' = \mathrm{d}r/\mathrm{d}t$ is the rate of the temporal decrease in the jet radius, v_{jet} is the flight speed of the jet, $L = 6.79 \times 10^{-20}$ J and $c_{\mathrm{p}} = 1.26 \times 10^{-22}$ J/K are the specific latent heat of vaporization and the specific heat capacity per a molecule, respectively, and k is the Boltzmann constant. The validity of Eq. (1) has been verified in [25] by Wilson and coworkers, where they compared $T(z)$ with the water jet temperature measured by laser Raman scattering. In our experimental condition, $r_0 = 25$ μm and $v_{\mathrm{jet}} = 13.6$ m/s. We employed $r' = 5.5$ mm/s by referring to the literature [25]. In this calculation, we ignored the heating power from the plasma to the water jet, since the heating power was estimated to be less than 1% of the cooling power due to the latent heat of vaporization. The flux of water vapor produced from the jet surface was estimated by

$$\Gamma_{\mathrm{H_2O}}(z) = \alpha \cdot \frac{1}{4}\frac{P_{\mathrm{H_2O}}(z)}{kT(z)}\sqrt{\frac{8kT(z)}{\pi M}}, \tag{2}$$

where $P_{\mathrm{H_2O}}(z)$ is the vapor pressure at $T(z)$ [26] and M is the mass of $\mathrm{H_2O}$. α denotes the ratio between the outward and inward fluxes of water vapor. We evaluated $\alpha = 0.43$ by comparing the production rate of water vapor calculated by Eqs. (1) and (2) with the experimental net production rate (80 μmol/s).

The variation in the production rate of water vapor calculated by Eqs. (1) and (2) is plotted in Fig. 3(a). As shown in the figure, the production rate calculated by Eqs. (1) and (2) was higher than that measured using QMS very slightly (the difference is below the magnitude of the error bars), indicating that almost all hydrogen and oxygen produced in the experiment

using the water jet were not originated from the consumption of water vapor. Therefore, it is possible to set up a hypothesis that the productions of hydrogen and oxygen are attributed to the oxidation and reduction, which are induced by the irradiation of the plasma, on the surface of the water jet. To confirm the redox reactions, we used the silver nitrate solution instead of pure water, and examined the production rates of hydrogen and oxygen. As a result, we observed a lower production rate of hydrogen, as shown in Fig. 4, and in contrast, the production rate of oxygen was the same as that observed using pure water. In addition, we observed cream-colored ice in the tank at the bottom of the chamber. We filtered the solution which was obtained by the melting of the cream-colored ice using a laboratory tissue paper and transferred the sample to a scanning electron microscope (SEM). Figure 5 shows the SEM image of the sample, together with the map showing the element distribution which was obtained by energy dispersive X-ray spectroscopy (EDS). We observed the production of particulates in the silver nitrate solution, as shown in Fig. 5(a). The EDS map shown in Fig. 5(b) indicates that they are silver particulates. This result clearly indicates the reduction of Ag^+ in the silver nitrate solution by immersing it in the plasma. The lower production rate of hydrogen in the silver nitrate solution, which is shown in Fig. 4, suggests the competition between the reductions of H^+ and Ag^+. The hypothesis of the redox reactions on the surface of the water jet has been thus approved by the comparative experiments.

The productions of hydrogen and oxygen in the experiment using the water vapor injection, which are shown in Fig. 3(b), can be explained by the conversion from water vapor ($2H_2O \rightarrow 2H_2 + O_2$), since the production rate of hydrogen is approximately equal to the loss rate of water vapor. The half of the production rate of hydrogen was slightly higher than the production rate of oxygen, and the difference may be due to the different pumping speeds for oxygen and hydrogen (Note that the production rate evaluated by the experiment is the "net" production rate). The first step in the production process is considered to be electron impact dissociation of H_2O. The collision with the metastable state of helium may partly contribute to the dissociation of H_2O, but the rate of the Penning dissociation is probably negligible since the loss rate of water vapor is proportional to the plasma density. Since three-body reactions are not expected at the pressure of 12 mTorr in the experiment, hydrogen and oxygen are likely produced by surface reactions on the chamber wall from dissociated species.

On the other hand, the experimental results shown in Figs. 3(a), 4, and 5 suggest the oxidation and reduction on the surface of the water (or the solution) jet immersed in the plasma, since hydrogen and oxygen were produced without consuming water vapor and the production of hydrogen was in the competition with the reduction of Ag^+ when the silver nitrate solution was used in stead of pure water. The production processes in the water jet experiment are considered to be

$$2H_2O \rightarrow O_2 + 4H^+ + 4e, \tag{3}$$

$$4H_2O + 4e_p \rightarrow 2H_2 + 4OH^- \tag{4}$$

and

$$4He^+ + 4e \rightarrow 4He, \tag{5}$$

where e_p denotes electron transported from the plasma. He^+ transported from the plasma oxidizes H_2O to form O_2 and H^+, which is the combination of reduction reaction (5) and oxidation reaction (3). The electron transported from the plasma reduces H_2O to form H_2 and OH^- (reaction (4)). Note that the electron and ion fluxes are equal in this experiment since the water jet is electrically floating. This means that we can expect the twice amount of H_2 production as compared with O_2. By summing up reactions (3)-(5), the overall reaction can be written as

$$2H_2O + 4He^+ + 4e_p \rightarrow 2H_2 + O_2 + 4He. \tag{6}$$

Note that H^+ produced in reaction (3) and OH^- produced in reaction (4) recombine to be H_2O. This redox reaction has two peculiar features. One is that both the oxidation and reduction occur simultaneously on the same water surface with no current. This is significantly different from a usual redox reaction system where the anode is separated from the cathode and a power supply is used for transferring electrons between the anode and the cathode. The other peculiar feature is its nonequilibrium nature. The normal reaction after the arrivals of He^+ and e_p on the water surface is the neutralization ($He^+ + e_p + H_2O \rightarrow He + H_2O$) since the energy state of the products is minimum. However, what we observed experimentally is that a part of the ionization energy of He (24.6 eV) is used for converting H_2O to H_2 and O_2 (the redox potential is 1.23 eV). This is an analogy with water decomposition using photocatalysts, where an electron and a hole work for the reduction and the oxidation of H_2O, respectively. Note that we detected hydrogen peroxide (H_2O_2) in the ice stored in the tank at the bottom of the chamber. The production of H_2O_2 may be owing to the reaction [3, 27, 28]

$$2H_2O \rightarrow H_2O_2 + 2H^+ + 2e. \tag{7}$$

H_2 is produced additionally from H^+ in reaction (7), which may explain the experimental result that the half of the production rate of hydrogen is higher than the production rate of oxygen.

The aforementioned production processes of hydrogen and oxygen have quantitative difficulty in the absolute production rates. If we assume a Bohm sheath between the plasma and the water jet, the fluxes of electrons and ions toward the water jet surface are

$$\Gamma_{He^+} = \Gamma_{e_p} = 0.61 n_p u_B, \tag{8}$$

where n_p is the plasma density and u_B is the Bohm velocity given by $u_B = \sqrt{kT_e/M_i}$ with T_e and M_i being the electron temperature and the ion mass, respectively. The surface area of the water jet is 1.6×10^{-6} m^2 if we assume a cylinder with a diameter of 50 μm and a length of 10 mm. Hence, the total number of electron-ion pair arriving at the water jet surface at a plasma density of $n_p = 2 \times 10^{16}$ m^{-3} is estimated to be 3.1×10^{-10} mol/s, which is five orders of magnitude lower than the production rates of hydrogen and oxygen. The huge difference would be compensated by the redox reactions on the surfaces of water droplets in the plasma chamber. The flow rate of water in the experiment was 1.6 mL/min or 2.7×10^{-8} m^3/s. Since the volume of the water jet with the length of 10 mm is 2.0×10^{-11} m^3, it is understood that almost all water injected into the plasma chamber does not keep the form of the jet and it is dispersed into droplets due to the Rayleigh instability [21, 25, 29]. We actually observed

the Mie scattering of visible light in the chamber, indicating the existence of droplets. If we assume ~ 1 μm and ~ 1 s for the diameter and the residence time of droplets in the plasma, respectively, the total surface area of droplets can explain the production rates of hydrogen and oxygen shown in Fig. 3(a). We speculate that the residence time of ~ 1 s is possible for droplets since they have negative charges and are trapped in the plasma. Note that the vaporization of droplets is negligible because of the low temperature.

In summary, we observed the productions of molecular hydrogen and molecular oxygen when a water jet was immersed in an inductively coupled helium plasma. The water jet was electrically floating, and no current was supplied from the plasma. The consumption of water vapor was negligible. The production of silver particulates was in competition with the production of hydrogen when we used a silver nitrate solution instead of water. These experimental results suggest that oxidation and reduction of water are the production processes of oxygen and hydrogen, respectively. The surface area of the water jet was significantly insufficient to explain the production rates, but it may be compensated by the surfaces of water droplets stored in the plasma. The reactions we observed are peculiar in the simultaneous oxidation and reduction at the same plasma-liquid interface by utilizing a part of the ionization potential of helium to fill the redox potential of water.

Acknowledgments

The authors are grateful to Naoki Shirai for valuable discussion. This work was supported by JSPS KAKENHI (20H00135). The SEM/EDS analysis was carried out in the laboratory of XPS analysis at joint-use facilities of Hokkaido university.

References

[1] Bruggeman P J, Frontiera R R, Kortshagen U R, Kushner M J, Linic S, Schatz G C, Andaraarachchi H, Exarhos S, Jones L O, Mueller C M, Rich C C, Xu C, Yue Y and Zhang Y 2021 Plasma-driven solution electrolysis *J. Appl. Phys.* **129** 200902

[2] Oldham T, Chen M, Sharkey S, Parker K M and Thimsen E 2020 Electrochemical characterization of the plasma-water interface *J. Phys. D: Appl.* **53** 165202

[3] Volkov A G, Bookal A, Hairston J S, Roberts J, Taengwa G and Patel D 2021 Mechanisms of multielectron reactions at the plasma/water interface: Interfacial catalysis, RONS, nitrogen fixation, and plasma activated water *Electrochimica. Acta.* **385** 138441

[4] Chen Q, Saito K, Takemura Y and Shirai H 2008 Physicochemistry of the plasma-electrolyte solution interface *Thin Solid Films* **516** 6688

[5] Richmonds C, Witzke M, Bartling B, Lee S W, Wainright J, Liu C-C and Sankaran R M 2011 Electron-transfer reactions at the plasma-liquid interface *J. Am. Chem. Soc.* **133** 17582

[6] Witzke M, Rumbach P, Go D B and Sankaran R M 2012 Evidence for the electrolysis of water by atmospheric-pressure plasmas formed at the surface of aqueous solutions *J. Phys. D: Appl. Phys.* **45** 442001

[7] Delgado H E, Radomsky R C, Martin D C, Bartels D M, Rumbach P and Go D B 2019 Effect of competing oxidizing reactions and transport limitation on the Faradaic efficiency in plasma electrolysis *J. Electrochem. Soc.* **166** E181

[8] Liu J, He B, Chen Q, Li J, Xiong Q, Yue G, Zhang X, Yang S, Liu H and Liu Q H 2016 Direct synthesis of hydrogen peroxide from plasma-water interactions *Sci. Rep.* **6** 38454

[9] Gopalakrishnan R, Kawamura E, Lichtenberg A J, Lieberman M A and Graves D B 2016 Solvated electrons at the atmospheric pressure plasma 寰努 ater anodic interface *J. Phys. D: Appl. Phys.* **49** 295205
[10] Kaneko T and Hatakeyama R 2018 Controlled gas 寰斗 iquid interfacial plasmas for synthesis of nano-bio-carbon conjugate materials *Jpn. J. Appl. Phys.* **57** 0102A6
[11] Richmonds C and Sankaran R M 2008 Plasma-liquid electrochemistry: Rapid synthesis of colloidal metal nanoparticles by microplasma reduction of aqueous cations *Appl. Phys. Lett.* **93** 131501
[12] Saito N, Hieda J and Takai O 2009 Synthesis process of gold nanoparticles in solution plasma *Thin Solid Films* **518** 912
[13] Tokushige M, Yamanaka T, Matsuura A, Nishikiori T and Ito Y 2009 Synthesis of magnetic nanoparticles (Fe and FePt) by plasma-induced cathodic discharge electrolysis *IEEE Trans. Plasma Sci.* **37** 1156
[14] Shirai N, Uchida S and Tochikubo F 2014 Synthesis of metal nanoparticles by dual plasma electrolysis using atmospheric dc glow discharge in contact with liquid *Jpn. J. Appl. Phys.* **53** 046202
[15] Shirai N, Yoshida T, Uchida S and Tochikubo F 2017 Synthesis of magnetic nanoparticles by atmospheric-pressure glow discharge plasma-assisted electrolysis Jpn. J. Appl. Phys. **56** 076201
[16] Yamazaki Y, Shirai N, Nakagawa Y, Uchida S and Tochikubo F 2018 Chemical reaction process for magnetite nanoparticle synthesis by atmospheric-pressure DC glow-discharge electrolysis *Jpn. J. Appl. Phys.* **57** 096203
[17] Liu J, Shirai N and Sasaki K 2021 Synthesis mechanism of cuprous oxide nanoparticles by atmospheric-pressure plasma electrolysis *J. Phys. D: Appl. Phys.* **54** 105201
[18] Kondeti V S Santosh K, Gangal U, Yatom S and Bruggeman P J 2017 Ag^{+} reduction and silver nanoparticle synthesis at the plasma-liquid interface by an RF driven atmospheric pressure plasma jet: Mechanisms and the effect of surfactant *J. Vac. Sci. Technol. A* **35** 061302
[19] Skiba M, Pivovarov A, Vorobyova V, Derkach T and Kurmakova I 2019 Plasma-chemical formation of silver nanoparticles: the silver ions concentration effect on the particle size and their antimicrobial properties *J. Chem. Technol. Metall.* **54** 2
[20] Shirai H, Nguyen M T, Čempel D, Tsukamoto H, Tokunaga T, Liao Y-C and Yonezawa T 2017 Preparation of Au/Pd bimetallic nanoparticles by a microwave-induced plasma in liquid process *Bull. Chem. Soc. Jpn.* **90** 279
[21] Kondow T and Mafuné F 2000 Structures and dynamics of molecules on liquid beam surfaces *Annu. Rev. Phys. Chem.* **51** 731
[22] Shreve A T, Yen T A and Neumark D M 2010 Photoelectron spectroscopy of hydrated electrons *Chem. Phys. Lett.* **493** 216
[23] Yamamoto Y, Karashima S, Adachi S and Suzuki T 2016 Wavelength dependence of UV photoemission from solvated electrons in bulk water, methanol, and ethanol *J. Phys. Chem. A* **120** 1153
[24] Riley J W, Wang B, Parkes M A and Fielding H H 2019 Design and characterization of a recirculating liquid-microjet photoelectron spectrometer for multiphoton ultraviolet photoelectron spectroscopy *Rev. Sci. Instrum.* **90** 083104
[25] Wilson K R, Rude B S, Smith J, Cappa C, Co D T, Schaller R D, Larsson M, Catalano T and Saykally R J 2004 Investigation of volatile liquid surfaces by synchrotron x-ray spectroscopy of liquid microjets *Rev. Sci. Instrum.* **75** 725
[26] NIST Chemistry webbook https://webbook.nist.gov/
[27] Wang L, Jiang X and Liu Y 2008 Degradation of bisphenol A and formation of hydrogen peroxide induced by glow discharge plasma in aqueous solutions *J. Hazard. Mater.* **154** 1106
[28] Konchekov E M, Glinushkin A P, Kalinitchenko V P, Artem'ev K V, Burmistrov D E, Kozlov V A and Kolik L V 2021 Properties and use of water activated by plasma of piezoelectric direct discharge *Front. Phys.* **8** 616385
[29] Charvat A, Lugovoj E, Faubel M and Abel B 2004 New design for a time-of-flight mass spectrometer with a liquid beam laser desorption ion source for the analysis of biomolecules *Rev. Sci. Instrum.* **75** 1209

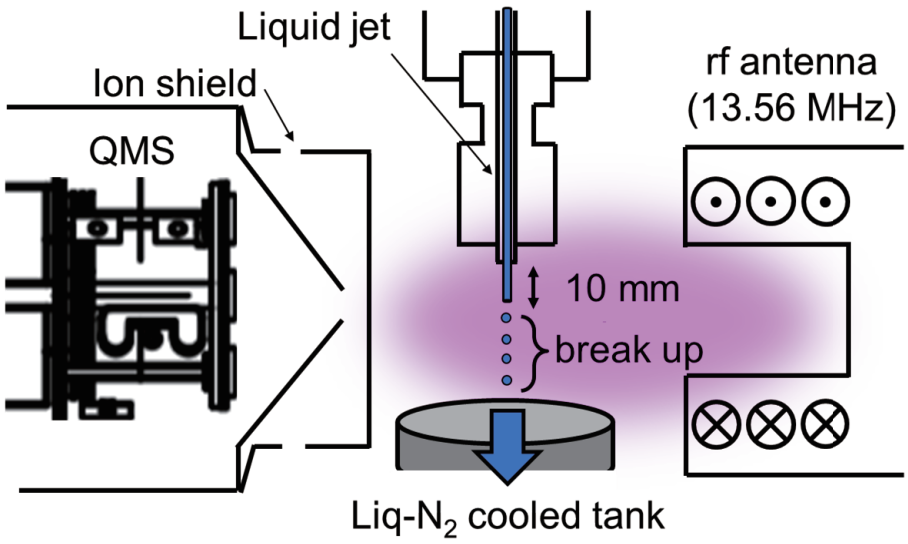

Figure 1. Experimental apparatus.

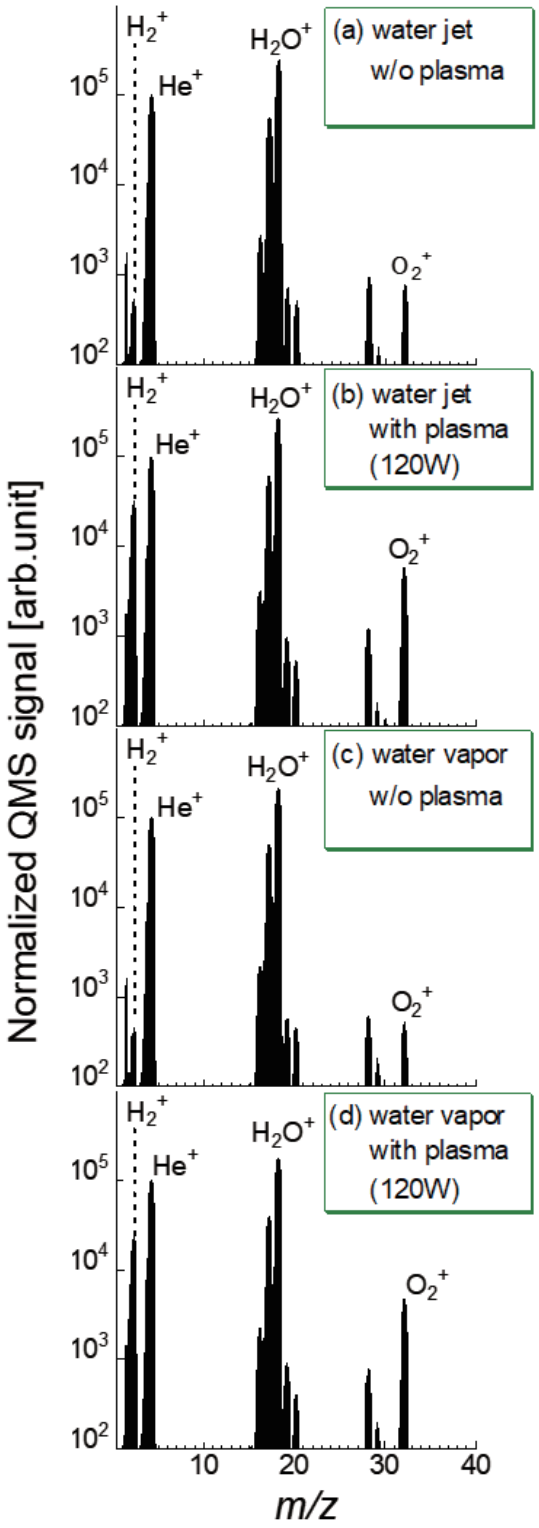

Figure 2. Examples of mass spectra. (a) and (b) were observed in the absence and presence of the plasma when the water jet was injected into the chamber, respectively. (c) and (d) were observed when only water vapor was introduced into the chamber.

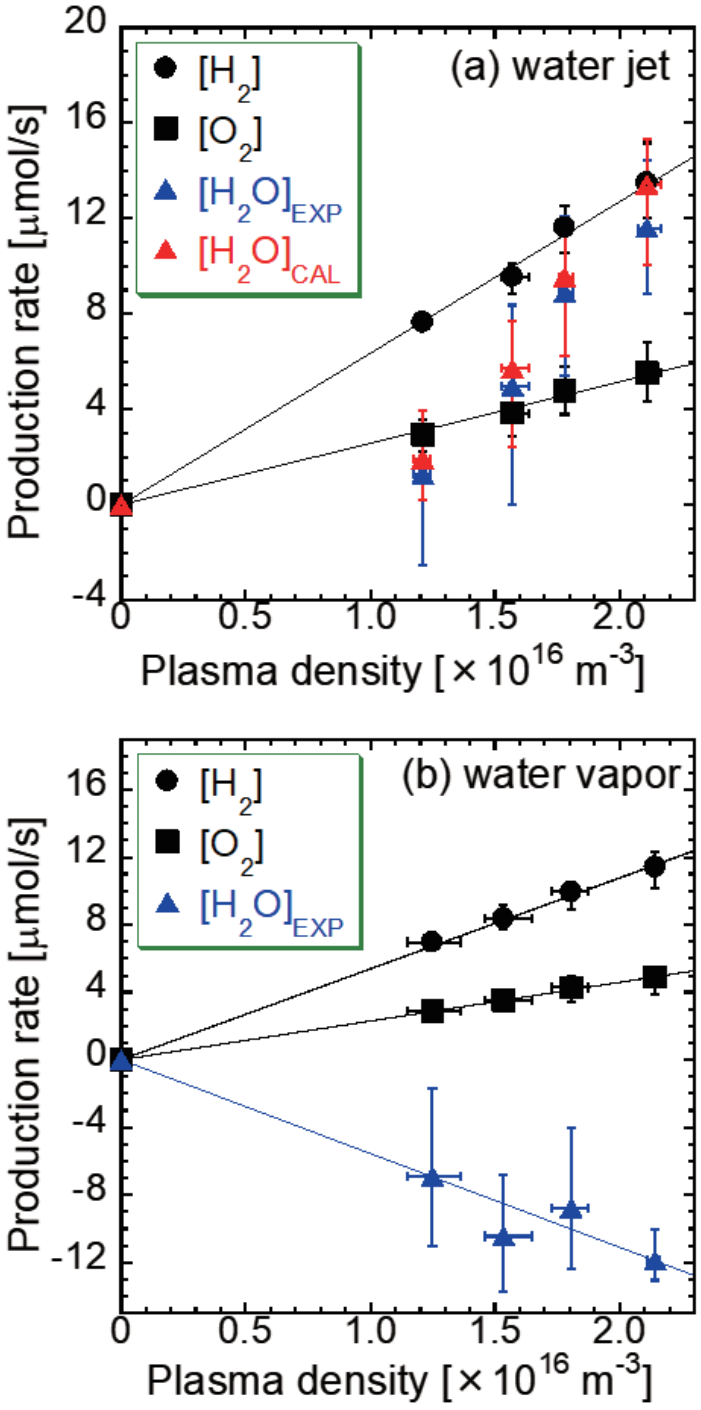

Figure 3. Relationship between the production rates of H_2, O_2 and H_2O and the plasma density (a) in the water jet experiment and (b) in the water vapor experiment.

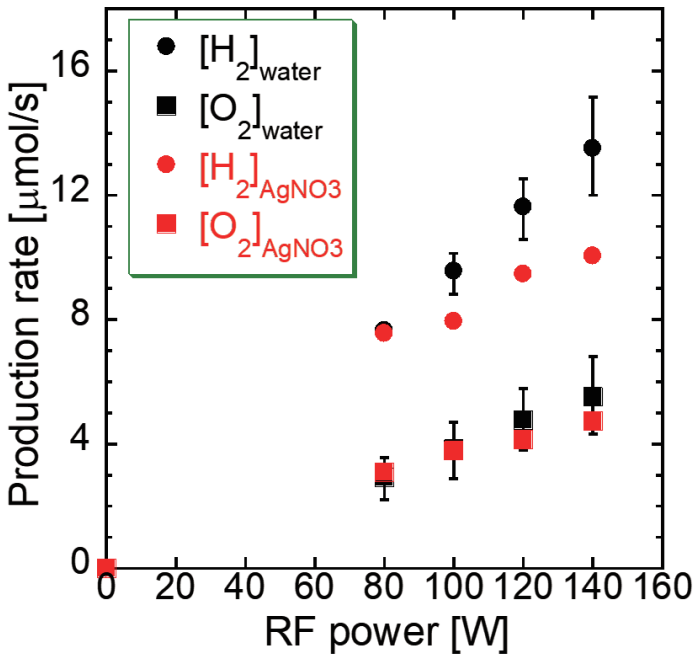

Figure 4. Production rates of H_2 and O_2 observed using silver nitrate solution were compared with those observed using pure water.

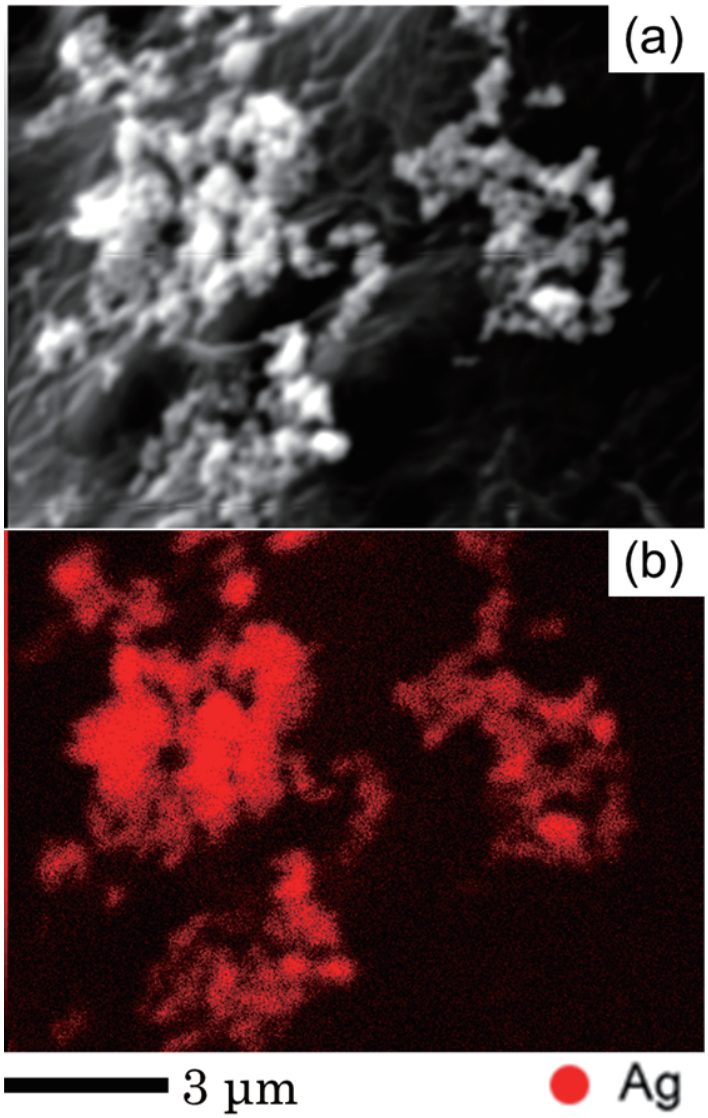

Figure 5. (a) SEM image and (b) silver EDS map of particulates produced by immersing silver nitrate solution in helium plasma.